## Locating the Ising CFT via the ground-state energy on the fuzzy sphere

## Kay Jörg Wiese

CNRS-Laboratoire de Physique de l'Ecole Normale Supérieure, PSL Research University, Sorbonne Université, Université Paris Cité, 24 rue Lhomond, 75005 Paris, France.

We locate the phase-transition line for the Ising model on the fuzzy sphere from a finite-size scaling analysis of its ground-state energy. Our strategy is to write the latter as  $E_{\rm GS}(N_m)/N_m=E_0+E_1/N_m+E_{3/2}/N_m^{3/2}+...$ , and to search for a minimum of  $\chi:=E_{3/2}/E_0$  as a function of the couplings. Conformal perturbation theory predicts that around a CFT,  $\chi=\chi_{\rm min}+\sum_i\lambda_i^2N_m^{-\omega_i}+\mathcal{O}(\lambda^3)$ , where  $\lambda_i$  are the couplings associated to perturbations of operators with dimension  $\Delta_i$ , and  $\omega_i=d-\Delta_i$ . This procedure finds the critical curve of [PRX 13 (2023) 021009] and their sweet spot with good precision. Varying two coupling constants allows us to extract  $\omega$  associated to the two leading scalars  $\varepsilon$ , and  $\varepsilon'$ . We find similar results when normalizing by the gap to the stress tensor T or first parity-odd operator  $\sigma$  instead of  $E_0$ .

### I. INTRODUCTION

The fuzzy-sphere regularization is an exciting new tool [1] to access conformal field theories (CFTs) in dimension d=2+1. The technique uses a 2-sphere inside which are placed s magnetic monopoles. The lowest Landau level on this sphere is  $N_m=2s+1$  times degenerate, each with  $N_{\rm f}$  flavors ( $N_{\rm f}=2$  for the Ising model). Filling  $N_m$  of the  $N_m \times N_{\rm f}$ states, and adding interactions between the electrons, allows one to engineer CFTs with a given symmetry. This approach was introduced in [1] to study the quantum 2d Ising model, equivalent to the classical 3d model. It was since applied to other systems, among which are theories with global Sp(n)[2] or O(3) [3] symmetry, Majorana fermions [4], a free scalar [5], Chern-Simons matter [6], the Potts model [7], and Yang-Lee [8-10]. The latter example is interesting as the theory is non-unitary, even though its spectrum is real; thus it is not accessible via the numerical conformal bootstrap [11–15] which is the current gold standard for 3d CFTs.

While the method allows one to study phases as well as critical points, the latter are particularly interesting, especially when they correspond to a CFT. A crucial step is to identify the location of the critical point. The standard approach consists in choosing couplings which optimize properties of the intended CFT, as the integer spacing of descendents [1]. Doing so without assuming what one wants to show is critical. There are interesting recent proposals [16, 17] to construct the conformal generators on the fuzzy sphere, allowing one to check for the overlap of states expected to be descendants, with the constructed descendants of expected primaries.

Here we locate the phase-transition line and sweet spot for the Ising model on the fuzzy sphere from a finite-size scaling analysis of the ground-state (GS) energy, without using any information on higher excited states. Our procedure finds the critical curve of [1] with good precision, and their sweet spot (point of optimal conformality) as well.

# II. SIZE-DEPENDENCE OF THE GROUND STATE ENERGY

In dimension d=2, the free energy per site of a classical CFT on a torus of circumference L is given by [18, 19],

$$f(L) = f_{\infty} - \frac{\pi c}{6L^2} + \mathcal{O}(L^{-3}). \tag{1}$$

Here  $f_{\infty}(L)$  is the free energy per site in the limit of  $L \to \infty$ , and c its central charge. This formula is valid at the critical point, and can be used to locate it: first one measures an effective central charge  $c_{\rm eff}(g|L)$ , where g is a microscopic coupling, via a fit to Eq. (1); then one demands that the theory is at a marginal point for  $c_{\rm eff}(g|L)$ [20],

$$\partial_g c_{\text{eff}}(g|L)\big|_{g=g^*} = 0 \implies \lim_{L \to \infty} c_{\text{eff}}(g^*|L) = c.$$
 (2)

For a standard (real) CFT, a local maximum for  $c_{\rm eff}(g|L)$  indicates a critical point, while a minimum indicates a critical phase. If the model at  $g^*$  is a CFT, then  $c_{\rm eff}(g^*|L)$  converges for  $L \to \infty$  to the central charge of the corresponding CFT.

The central charge has three properties: (i) it appears in the Virasoro algebra of conformal generators, (ii) it governs finite-size corrections as in Eq. (1), and it decreases along the RG flow (Zamolodchikov's c-theorem [21]). This motivates the condition (2) for fixed points, and explains why a critical point is a local maximum. The marginality condition (1) can also be used for complex CFTs, and allowed the authors of [20] to locate the critical point of the 5-state Potts model in d=2, which has a complex second derivative, thus is neither maximum nor minimum.

There is a generalization of Zamolodchikov's c-theorem to d=4, related to anomalies under Weyl rescaling [22, 23], which gives the stress-energy tensor in the form (see Eq. (1.2) of [24])

$$T^{\mu}_{\mu} = aE_4 - cW^2_{\mu\nu\rho\sigma}.\tag{3}$$

Here  $E_4$  is the Euler density (which integrates to the Euler characteristic), and W the Weyl tensor. It was first conjectured and checked to 1-loop order by Cardy [25], and later proven in [24] that a decays along RG trajectories (a-theorem).

We now consider dimension d=3. Ref. [26] (section 1) considers finite-size corrections for the free energy of an Euclidean field theory on a 3-sphere of radius R imbedded into  $\mathbb{R}^4$ ,

$$F = -\ln|Z_{S^3}| = \alpha_0 R^3 + \alpha_1 R + \mathcal{F}.$$
 (4)

While  $\alpha_0$  and  $\alpha_1$  are non-universal, the last term  $\mathcal{F}$  is a number, and may contain universal information.  $\mathcal{F}$  was first obtained via holography [27] and in super-symmetric models

[28], and only later for more general theories [29]. It took some time to find a proper definition which is universal, and independent of the microscopic degrees of freedom [30, 31]. Currently, the best approach to extract  $\mathcal{F}$  is to study the entanglement spectrum [32]. Refs. [31, 32] proved that  $\mathcal{F}$  so defined descends along the RG flow. Ref. [33] succeeded to extract  $\mathcal{F}$  from the entanglement entropy on the fuzzy-sphere realization of the Ising model.

Now consider the free energy on  $\mathbb{R}^3 \simeq \mathcal{S}_2 \times \mathbb{R}$ , where the r.h.s. is the geometry used in the fuzzy-sphere approach. To pass to the left, Euclidean time  $\tau$  is mapped as  $\tau \to \mathrm{e}^\tau$ , with  $\tau \in [-\beta/2, \beta/2]$ . For  $\beta \gg R$ , we expect the free energy to be

$$F = -\ln Z = \beta \left[ \alpha_0 R^2 + \alpha_1 + \frac{\alpha_{3/2}}{R} + \dots \right].$$
 (5)

The coefficient which may contain universal information is  $\alpha_{3/2}$ , as it is the only one without a scale. We can pass to the quantum problem by taking  $\beta \to \infty$ ,

$$E_{\rm GS}(R) = v_{\rm F} \left[ \alpha_0 R^2 + \alpha_1 + \frac{\alpha_{3/2}}{R} + \dots \right].$$
 (6)

Here  $v_{\rm F}$  is un unknown Fermi velocity, which in general depends on the microscopic couplings.

Let us explain why we did not include a term of order R into  $E_{\rm GS}(R)$ : the two leading terms in the vacuum energy allowed by geometry and necessitating counter-terms (CT) are

$$E_{\text{GS}}^{\text{CT}}(R) = \int d^2x \sqrt{g} \Big( \mu + \kappa \mathcal{R} \Big),$$
 (7)

where R is the radius of the sphere,  $\mathrm{d}^2 x \sqrt{g}$  the invariant measure,  $\mu$  the coefficient of the vacuum-energy density ("cosmological constant"), and  $\kappa$  the coefficient multiplying the curvature  $\mathcal{R}$ . According to the Gauß-Bonnet theorem, the latter integrates to  $4\pi\chi$ , where  $\chi$  is the Euler characteristic;  $\chi=2$  for a sphere. As a result  $E_{\mathrm{GS}}^{\mathrm{CT}}(R)=4\pi R^2\mu+8\pi\kappa$ .

Using the identification that the area of the sphere grows as the number of electrons, or more precisely [34]

$$N_m^2 = 1 + 4R^4, (8)$$

we get for the GS energy per electron<sup>1</sup>

$$\frac{E_{\rm GS}(N_m)}{N_m} = E_0 + \frac{E_1}{N_m} + \frac{E_{3/2}}{N_m^{3/2}} + \dots$$
 (9)

We recall that physical information is expected in  $E_{3/2}$ . This is in line with the observation that the gap of any excited state has the same scaling in  $N_m$  as  $E_{3/2}$  (for the stress-energy gap  $E_T - E_{\rm GS}$  see discussion below and Fig. 9); thus if one looks for a coefficient of the GS energy which is universal, one again concludes that the only viable candidate is  $E_{3/2}$ .

At this point it is interesting to recall a standard tool in data analysis, the Binder cumulant a.k.a. kurtosis (ratio of fourth moment divided by the square of the second moment). In the vicinity of a phase transition, it takes the form

$$\mathcal{B}(\{\lambda_i\}|R) = \mathcal{B}_0 + p(\{\lambda_i R^{-\omega_i}\}), \qquad \omega_i = \Delta_i - d, \quad (10)$$

where  $\mathcal{B}_0$  is a number, and p a function<sup>2</sup> in the couplings  $\lambda_i$  associated with perturbations by operators of dimension  $\Delta_i$ . We postulate that  $E_{3/2}$  can play a similar role to the Binder cumulant in locating the point where finite-size corrections are minimized.

Now consider the behavior close to a CFT. There the action takes the form

$$S = S^{CFT} + \sum_{i} \lambda_{i} \int_{x} \mathcal{X}_{i}(x), \tag{11}$$

where  $\mathcal{X}_i(x)$  are primaries. Schematically, the free energy in statistical field theory is [35]

$$F = -\ln Z = F_0^{\text{CFT}} + \sum_i \lambda_i \int_x \langle \mathcal{X}_i(x) \rangle_{\text{CFT}}$$
$$-\frac{1}{2} \sum_{i,j} \int_{x_1} \int_{x_2} \langle \mathcal{X}_i(x_1) \mathcal{X}_j(x_2) \rangle_{\text{CFT}}^{\text{c}} + \dots \quad (12)$$

As the vacuum expectation of primaries vanishes, the linear terms are absent. At second order, only the term with i=j survives. The result is

$$F = F_0^{\text{CFT}} - \sum_i \left( \lambda_i R^{d - \Delta_i} \right)^2. \tag{13}$$

We have not specified our domain of integration, and absorbed possible geometrical factors into  $\lambda_i$ . Eq. (13) has a factor of  $R^{2d}$  from the integration measure, and a factor of  $R^{-2\Delta_i}$  from the 2-point function  $\langle \mathcal{X}_i(0)\mathcal{X}_i(R)\rangle = R^{-2\Delta_i}$ . An equivalent procedure can be performed in the quantum-formulation [36, 37] which uses the sphere as geometry<sup>3</sup>. We conclude that

$$E_{3/2} = E_{3/2}^{\text{CFT}} - \sum_{i} (\lambda_i R^{d-\Delta_i})^2 + \mathcal{O}(\lambda_i^3).$$
 (14)

A cubic term is expected as there are non-vanishing 3-point functions. Eq. (14) is of the form postulated in Eq. (10). In order to eliminate the Fermi-velocity  $v_{\rm F}$  in Eq. (6), below we shall analyze<sup>4</sup>

$$\chi := \frac{E_{3/2}}{E_0}. (15)$$

(Alternative normalizations are discussed in section III G.) Since in our problem  $E_0$  is negative, a CFT implies a minimum of  $\chi$ . Around this minimum, we expect

$$\chi = \chi_{\min} + \sum_{i} \frac{\lambda_i^2}{N_m^{\omega_i}}, \quad \omega_i = \Delta_i - d.$$
 (16)

<sup>&</sup>lt;sup>1</sup> The GS energy given by FuzzifiED is indeed  $\sim N_m$ .

<sup>&</sup>lt;sup>2</sup> When a perturbative expansion in  $\lambda_i$  exists, p is a polynomial.

<sup>&</sup>lt;sup>3</sup> In this formulation, the integration measure gives  $R^{2d-2}$ . The seemingly missing factor of  $R^2$  is provided by the denominator  $E_i - E_{\rm GS} \sim R$ , correcting an energy  $\sim R$ . The quantum version with its well-defined geometry is appropriate for evaluating the geometrical prefactors.

<sup>&</sup>lt;sup>4</sup> If there are perturbative corrections to E<sub>0</sub>, we expect them to take the same form as in Eq. (14), so that the argument remains valid for the ratio.

As we show below, this procedure finds the critical curve and the sweet spot of [1] with good precision. The standard algorithm to locate a CFT is to search for a spectrum with integervalued spacing for descendants of primary operators, as dictated by CFT [1], or explicitly check for conformal symmetry [16, 17]. Our procedure is an alternative. Its sole ingredient is the GS energy. Its advantages are that it is simple to implement, and computationally fast.

# III. FINITE-SIZE SCALING ANALYSIS OF THE GROUND-STATE ENERGY

#### A. Model

We use the Ising model defined in the seminal work [1]. It consists of a 2-sphere with s magnetic monopoles at its center, onto which are placed  $N_m=2s+1$  fermions, each with two internal degrees of freedom (up and down spin). Without interactions, the spectrum is flat. One then introduces a repulsive interaction upon contact between electrons pointing in the z-direction of strength 1, and a "kinetic" term (coupling to the gradient of the density interactions) of strength  $g \equiv V_1$  in the same direction. Finally, a transverse magnetic field of strength h drives the phase transition, similar to what happens in the 1-dimensional spin chain.

#### B. FuzzifiED

We use the package FuzzifiED. It provides a compact and efficient implementation to obtain the spectrum of a user-defined model on the fuzzy sphere, both using exact diagonalization and DMRG. The package is described in detail in [34]. The program we used is an adaptation of "ising spectrum.jl", wrapped inside a Mathematica loop. To avoid numerical errors, we eliminated the rounding, i.e. the instruction "round.([enrg[i], 12\_val[i], P, Z], digits = 6)". For system sizes  $N_m \geq 16$  we restrict the evaluation to the GS energy, leading to a considerable speedup. (We can do  $N_m = 17$  in about 10 minute on 8 cores, using a machine from 2013.)

### C. Dependence of the GS energy on system size

We had motivated the ansatz (9) for the GS energy. In the rest of this work, we use this ansatz with two additional subleading terms,

$$\frac{E_{GS}(x|h,g)}{N_m} = E_0(h,g) + E_1(h,g)x + E_{3/2}(h,g)x^{\frac{3}{2}} + E_2(h,g)x^2 + E_{5/2}(h,g)x^{\frac{5}{2}} + \dots \quad (17)$$

$$x := \frac{1}{N_m}.$$
(18)

Let us check this against exact diagonalization. Fig. 1 shows that the GS<sup>1</sup> has both a constant  $E_0$  and a strong linear component  $E_1$ . We tried adding a term of order  $\sqrt{x}$  and found that

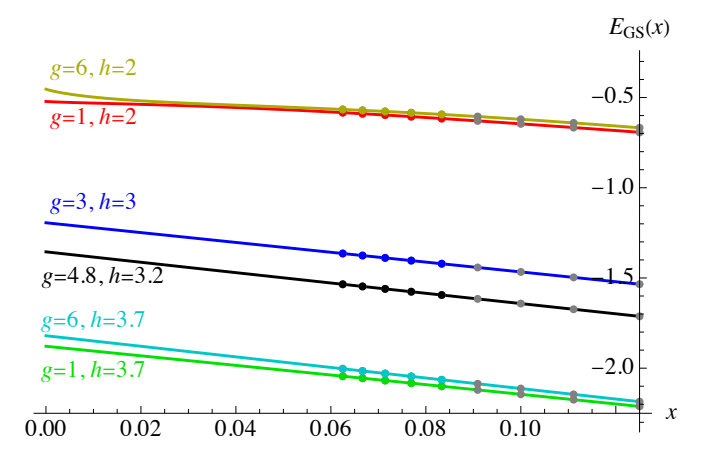


FIG. 1.  $E_{\rm GS}(x)$  for various values of h and g, for o=4, using  $x^{i/2}$  as a basis,  $\{1,x,x^{3/2},x^2,x^{5/2}\}$ ,  $N_m^{\rm max}=16$ . Gray dots are not used for the fit, but in agreement with it.

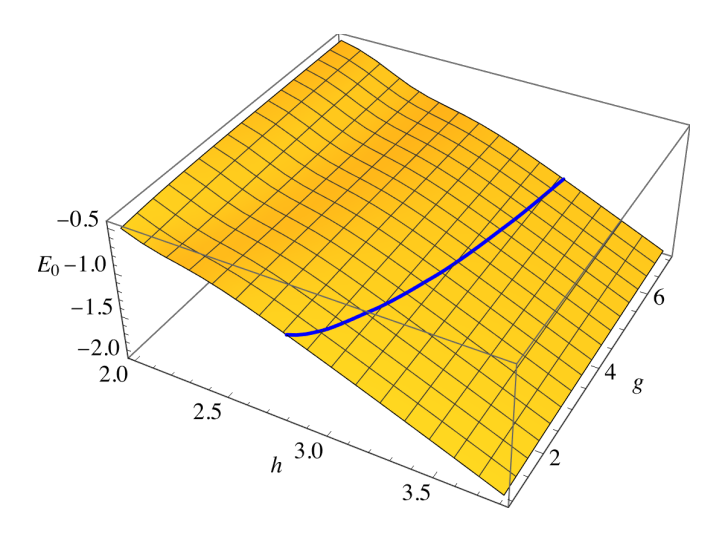


FIG. 2.  $E_0=E_{\rm GS}(0|h,g)$  for o=4,  $N_m^{\rm max}=16$ ; this plot changes little between  $N_m^{\rm max}=13$  and  $N_m^{\rm max}=16$ . In blue the critical line.

its coefficient is either absent or very small. Out of curiosity, we also tried an ansatz with integer coefficients. We found that information about the critical line can be extracted, but seems to be sitting in higher derivatives, which we do not find convincing, see appendix A. We also played with different orders of the truncation. We trust our analysis when higher-order coefficients are small. With its almost straight behavior, Fig. 1 (which uses Eq. (17)) suggests that the leading term in the expansion is indeed of order x, and not  $\sqrt{x}$ , or that at least the coefficient  $\sim \sqrt{x}$  is very small, and we discard it. Adding terms beyond  $E_{3/2}$  seems helpful (see appendix A).

We now look at the GS energy extrapolated to x=0. As Fig. 2 attests this is rather featureless. A crucial problem with quantum-mechanical approaches is that all energy levels are multiplied by an unknown Fermi velocity  $v_F$ , see Eq. (6). In the fuzzy-sphere approach, this is usually fixed by demanding that the stress-energy tensor have dimension d=3. An alternative is to prescribe the energy of the first excited state  $\sigma$  which suffers less from finite-size corrections close to the

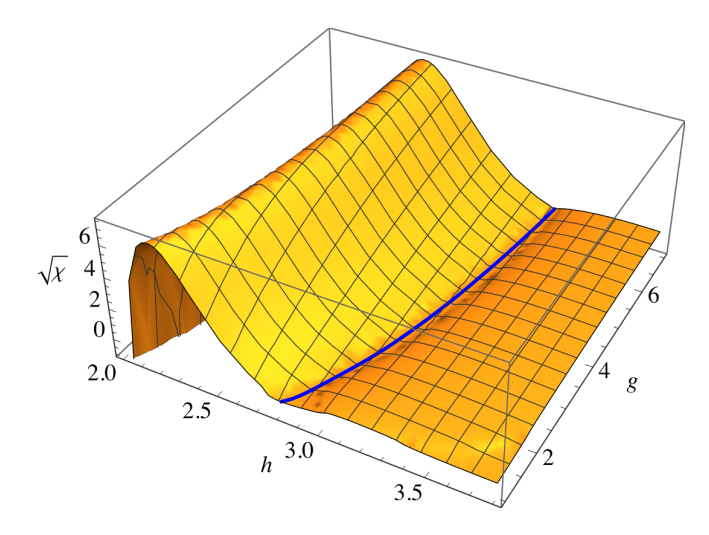


FIG. 3.  $\chi$  for  $N_m^{\rm max}=16$ ; in blue the critical line. To make the minimum visible, we plot the signed root  $(\sqrt{\chi}:={\rm sign}(\chi)\sqrt{|\chi|})$ . To enhance the resolution of the plot, the interpolation outlined below in Eq. (20) and Fig. 5 was used.

Ising CFT [37]. Our goal here is to extract the location of the CFT solely from the GS energy. To eliminate the unknown Fermi-velocity, we consider finite-size corrections normalized by the extrapolated GS energy, i.e.

$$\chi(h,g) := \frac{E_{3/2}(h,g)}{E_0(h,g)},\tag{19}$$

where the coefficients are those of Eq. (17). Alternative normalizations are discussed in section III G.

#### D. Implementation

Our ED data are such that we can use  $N_m=8$  to 17, i.e. a maximal  $N_m$  per fit of  $N_m^{\rm max}=12$  to 17. Large sizes are possible since we only need the GS energy. For the order of approximation, we tried o=2,3,4,5 and 6 (o counts the number of terms beyond the constant  $E_0$ ). Larger orders o are not necessarily better, as numerical artifacts are amplified in ways possibly not detectable. Common sense and experience lead us to consider o=4 optimal, i.e. the form given in Eq. (17).

We now evaluate  $\chi$ : following [1], we plot h on the horizontal axis, and g on the vertical axis. We first show a 3D plot, see Fig. 3, then a heat-plot on Fig. 4. On the latter, the critical line of [1] is given in white (partially hidden under blue dots), with a white shamrock marking their *sweet spot* (best agreement with Ising CFT). The dark blue dots in Fig. 4 mark the valley floor, defined as follows: look at the Hessian  $H_{ij} := \partial_i \partial_j \chi(h,g)$ , where  $i,j \in \{h,g\}$ . Since  $H_{ij}$  is symmetric, it has two eigenvalues, the curvatures, and two eigenvectors, which are orthogonal. We take the eigenvector in the direction of the larger curvature, and ask that the slope in this

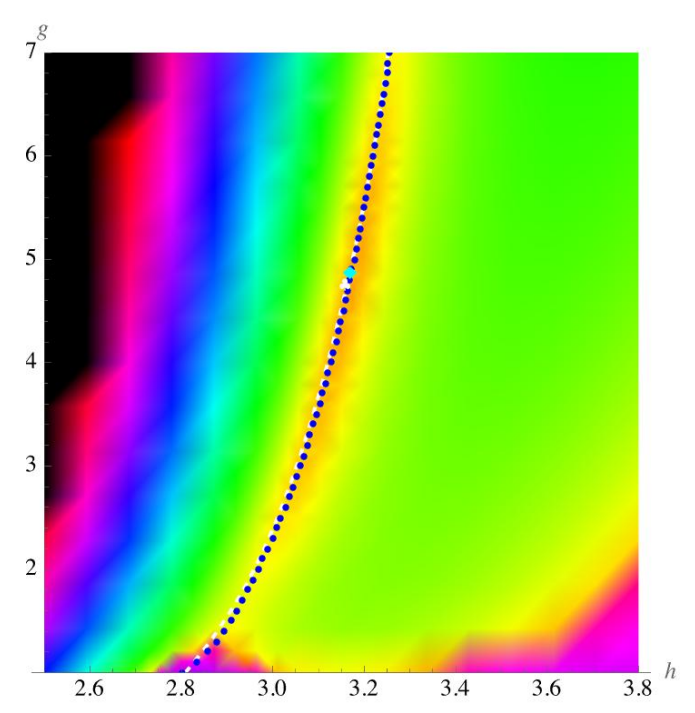


FIG. 4. Heat map of  $\chi(h,g)$  given in Eq. (15) for o=4,  $N_m^{\rm max}=16$ . The white dashed line is the critical line of [1], with a white shamrock marking their sweat spot (best agreement with a CFT). In dark blue dots the minimum of the valley of  $\chi(h,g)$ . The cyan diamond marks the global minimum of  $\chi(h,g)$ .

direction vanishes<sup>5</sup>.

This is a highly non-linear operation on the numerical data generated on a grid with step size  $\delta h=1/20,\,\delta g=1/5,$  for which we need a smooth interpolation. This is obtained by fitting a polynomial of maximal degree four (15 coefficients) to the  $6\times 6$  neighbors, weighted by

$$\rho(h,g) := \exp\left(-\alpha \left[ \frac{(h_i - h)^2}{\delta h^2} + \frac{(g_i - g)^2}{\delta g^2} \right] \right), \quad (20)$$

where  $\alpha=0.6$  is a phenomenological parameter. An example for the weights is given in Fig. 5. Compared to lattice-based approaches which are discontinuous when a new interpolation point enters, our procedure is very smooth. If the data turn out to be noisy, one can decrease  $\alpha$  to effectively include more points in the fit. The number of neighbors is chosen s.t. additional points have vanishing weight.

#### E. Results for the location of the critical point

As Fig. 4 attests, we can locate the phase-transition line of Ref. [1] which corresponds to the white dashed line. Our val-

<sup>&</sup>lt;sup>5</sup> This definition uses the metric of the coordinates h and g. It is not invariant under reparametrization, e.g.  $\{h,g\} \rightarrow \{h,g+h\}$ . The result is rather similar if we look at a vanishing slope in the h direction only; this we believe is what [1] did in their optimization procedure. Not knowing the metric will haunt as later, see section III F.

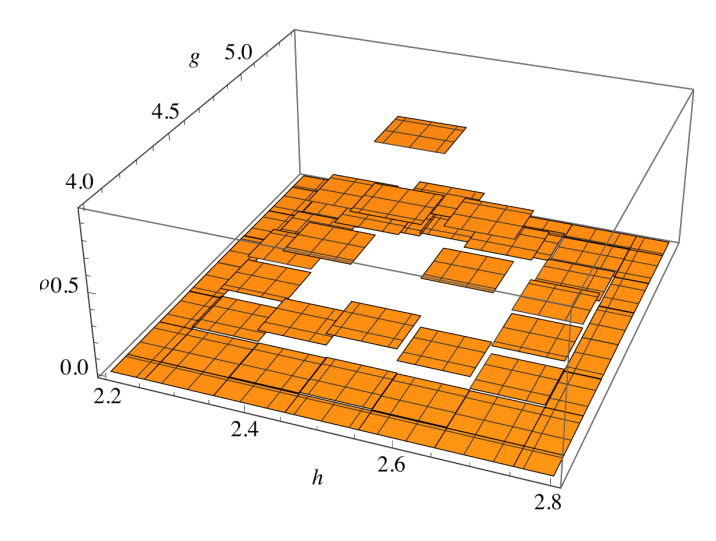


FIG. 5. The weights  $\rho(h,g)$  defined in Eq. (20), for h=2.5 and q = 4.75 (off grid).

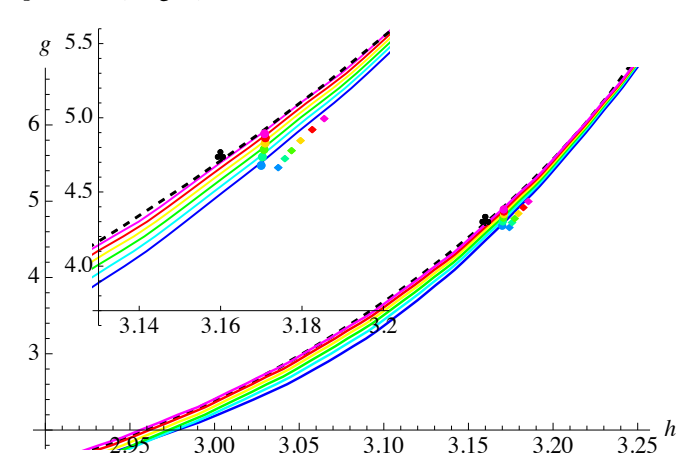


FIG. 6. Main plot: Dependence on  $N_m^{\rm max}$  of the critical curve and sweet spot (dots) from a grid with  $\delta g = 0.2$ ,  $\delta h = 0.05$ ; from  $N_m^{\text{max}} = 12$  (blue), over  $N_m^{\text{max}} = 13$  (cyan) to  $N_m^{\text{max}} = 17$  (magenta); diamonds mark the minimum on a micro-grid with discretization  $\delta g = 0.05$ ,  $\delta h = 0.01$ . The inset shows a blow-up around the sweet spot. Deviations are indicative of errors due to the finite grid size. In black dashed the critical line of [1], a black trefle marking its sweet spot.

ley of  $\chi(h,g)$  is marked by blue dots. On this phase-transition line the best agreement with the Ising CFT is achieved at the position of the white shamrock [1], while the nearby global minimum of  $\chi(h, g)$  is marked by a cyan diamond. The latter minimum satisfies

CFT: 
$$\partial_h \chi(h,g) = \partial_g \chi(h,g) = 0.$$
 (21)

How this minimum depends on the system size is shown in Fig. 6. There is a small systematic upwards drift on the minima obtained via interpolation (dots). We repeated the analysis on a much finer grid ("micro-grid") with  $\delta g = 0.05$  and  $\delta h = 0.01$  around the sweet spot, obtaining comparable results, see the diamonds on Fig. 6, and table 7.

$N_m^{\text{max}}$	h	g	$\chi_{ m min}$	$\chi''_{\rm max}$	$\chi''_{\min}$
12	3.17422	4.66314	0.0056442	10.97	0.01907
13	3.17587	4.72479	0.0054353	12.86	0.01188
14	3.17750	4.78087	0.0050100	14.88	0.00780
15	3.17965	4.84383	0.0045505	17.01	0.00599
16	3.18256	4.91919	0.0041134	19.27	0.00496
17	3.18553	4.99396	0.0037134	21.64	0.00441

FIG. 7. Values for the minimum of  $\chi$ , its location and the two eigenvalues of  $\chi'' = \partial_i \partial_j \chi$  with i, j = h, g for different  $N_m^{\text{max}}$ , obtained on a grid with  $\delta g = 0.05$ ,  $\delta h = 0.01$ .

### F. Curvature scaling

Eq. (16) states how  $\chi$  behaves close to its minimum. Since our numerical data are obtained with two parameters,  $\{h, g\}$ , we should see an approximation involving the two leading parity-even scalars  $\varepsilon$  and  $\varepsilon'$ :

$$\chi \simeq \chi_{\min} + \frac{\lambda_1^2}{N_m^{\omega_1}} + \frac{\lambda_2^2}{N_m^{\omega_2}},$$
(22)

$$\chi \simeq \chi_{\min} + \frac{\lambda_1^2}{N_m^{\omega_1}} + \frac{\lambda_2^2}{N_m^{\omega_2}}, \qquad (22)$$

$$\begin{pmatrix} \lambda_1 \\ \lambda_2 \end{pmatrix} = \mathbb{M} \begin{pmatrix} h - h_c \\ g - g_c \end{pmatrix}. \qquad (23)$$

The matrix M has four parameters. Two can be used for rescaling  $\lambda_1$  and  $\lambda_2$ ; since this only shifts the curves in plot 8 vertically, we discard it. The next parameter is for a rotation. Independent of  $N_m$ , we find a rotation by -0.046 radians  $(-2.7^{\circ})$ . As a result,  $h-h_{\rm c}$  strongly aligns with  $\lambda_1$ . On Fig. 8 we show how the largest and smallest eigenvalues of  $\chi'' := \partial_i \partial_j \chi$  with i, j = h, g (see Fig. 7) scale with  $N_m$ . This allows us to extract  $\omega_1 \approx -1.9$ , and  $\omega_2 \approx 2.7$  from the last two data points. We plot the successive slopes in the middle of Fig. 8. For  $\omega_1$  it allows us to extrapolate  $N_m \to \infty$ , resulting

$$\omega_1 \approx -1.60, \quad \omega_{\varepsilon} = \Delta_{\varepsilon} - 3 = -1.58738.$$
 (24)

This is close to the numerical bootstrap result [12] for  $\varepsilon$ .

It is more delicate to extract  $\omega_2$ , as the decreasing slope on the left plot in Fig. 8, shown in the middle plot, asserts. We still have one parameter left in M: it corresponds to an angle different from 90° between the microscopic coupling constants. To exploit this, a simple procedure is to write  $\chi$  to second order as

$$\tilde{\chi} = \chi_{\text{max}}'' \frac{\lambda_1^2}{2} + \chi_{\text{min}}'' \frac{\lambda_2^2 + \alpha \lambda_1 \lambda_2}{2},\tag{25}$$

and redo the scaling analysis of the data in Fig. 7 with the eigenvalues of  $\partial_i \partial_i \tilde{\chi}$ , optimizing  $\alpha$  s.t. the last three points for  $\omega_2$  lie on a straight line, see the right plot on Fig. 8. With the optimal  $\alpha = 59.868$  we find the last four points to align, which allows us to extract

$$\omega_2 \approx 0.94, \quad \omega_{\varepsilon'} = \Delta_{\varepsilon'} - 3 = 0.82968.$$
 (26)

This is now close to the prediction [12] from the numerical bootstrap for  $\varepsilon'$ . As we have exhausted our free parameters, we can not go further.

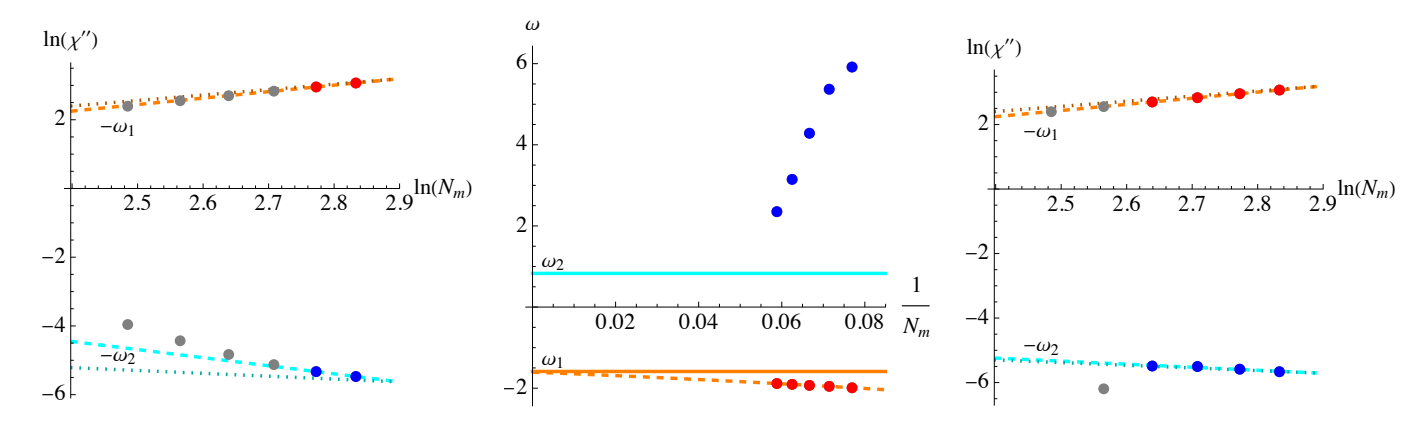


FIG. 8. Left: Scaling of the two eigenvalues of  $\partial_i\partial_j\chi$  (with i=h,g) w.r.t.  $N_m$ . The dashed lines are fits with  $\omega_1\approx-1.9$  and  $\omega_2\approx2.7$ , the dotted lines the expected slopes. Gray dots are not included into the fit. Middle: extrapolation of  $\omega_1$  and  $\omega_2$  to  $N_m=\infty$  (using a quadratic polynomial for  $\omega_1$ ). We find  $\omega_1\approx-1.60$  and  $\omega_2\approx1$ , to be compared to  $\omega_\varepsilon=\Delta_\varepsilon-3=-1.58738$ , and  $\omega_{\varepsilon'}=\Delta_{\varepsilon'}-3=0.82968$  (solid lines) [12]. Using a skew transformation to align the last three points for  $\omega_2$  (see text) gives  $\omega_1$  as before and  $\omega_2=0.94$ , now close to the expected results.

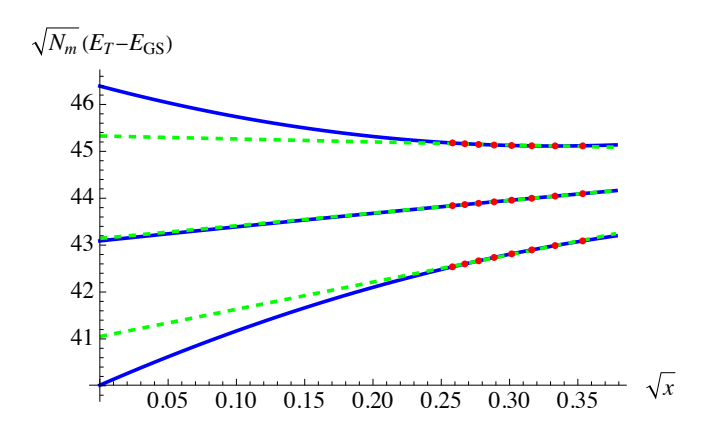


FIG. 9. The rescaled stress-energy tensor gap  $\sqrt{N_m}(E_T-E_{\rm GS})$  ( $\ell=2,\,P=Z=1$ ) close to the sweet spot: g=4.8 and h=3.1 (bottom), h=3.2 (middle), h=3.3 (top). Fits to  $\{1,\sqrt{x},x\}$  (blue), compared to a linear fit (dashed green line). Interestingly, the curvature changes sign at the transition.

#### G. Alternative normalizations

The alert reader will object that  $E_0$  is not universal<sup>6</sup>. We propose two ways out of this dilemma, which demand to calculate one more eigenvalue, either  $E_T$ , the subleading contribution in the GS sector corresponding to the stress-energy tensor, or  $E_\sigma$ , the lowest-lying parity-odd state.

Let us first consider  $E_T$ . On Fig. 9 we show how weakly  $E_T - E_{GS}$  depends on x. We found it appropriate to fit to  $\{1, \sqrt{x}, x\}$ . Interestingly, the curvature in  $\sqrt{x}$  changes sign at the transition; one should explore this further. Fig. 10 shows the resulting extrapolated value of the stress-energy gap as a

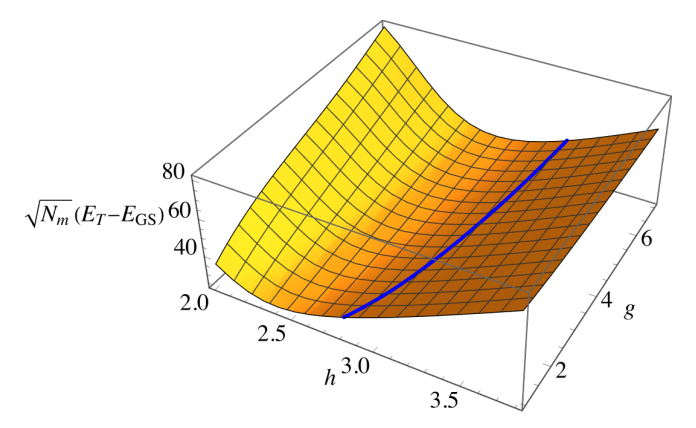


FIG. 10. The stress-energy tensor gap ( $\ell=2,\,P=Z=1$ ) multiplied by  $\sqrt{N_m}$ , and extrapolated to x=0. Fit to  $\{1,x^{1/2},x\}$ ,  $N_m^{\max}=15$ .

function of h and g. This allows us to define

$$\chi_T := \frac{E_{3/2}}{\sqrt{N_m}(E_T - E_{GS})}. (27)$$

A plot of this function is shown on Fig. 11, which should be compared to Fig. 3.

A second alternative is to normalize by the gap of the first parity-odd operator  $\sigma$ ,

$$\chi_{\sigma} := \frac{E_{3/2}}{\sqrt{N_m}(E_{\sigma} - E_{GS})}.$$
 (28)

While the  $\sigma$ -gap is rather insensitive to perturbations close to the Ising CFT [37], it depends strongly on h, as Fig. 12 attests. Trying to extrapolate to  $N_m = \infty$  even with a linear fit in  $\sqrt{x}$  and two consecutive system sizes leads to a non-sensical negative gap. For this reason, we use only one system size for the normalization in Eq. (28). The result is shown on Fig. 13, which should be compared to Figs. 3 and 11.

<sup>&</sup>lt;sup>6</sup> Our procedure continues to work as long as  $E_0(h,g) - E_0(h_c,g_c)$  has an expansion of the form (14).

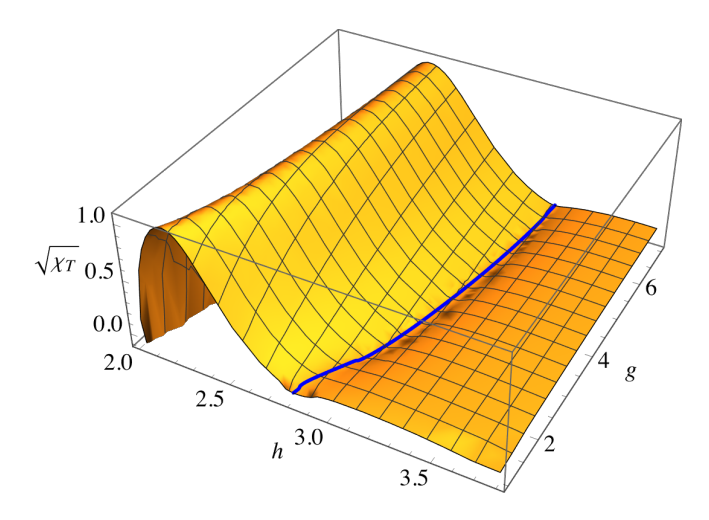


FIG. 11.  $\chi_T$  for  $N_m^{\rm max}=15$ ; in blue the critical line. We use the same approach as in Fig. 3 for  $\chi$ .

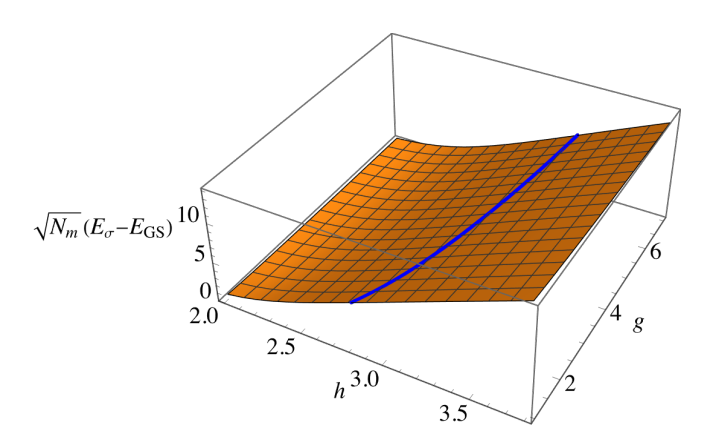


FIG. 12.  $\sqrt{N_m}(E_\sigma-E_{\rm GS})$  for  $N_m=15$ . Note that the gap vanishes for small h: one is in the non-critical ferromagnetic phase.

We now use  $\chi$ ,  $\chi_T$  and  $\chi_\sigma$  at  $N_m^{\rm max}=15$ , and repeat the analysis for the critical line and sweet spot. Fig. 14 shows this comparison, for a slightly coarser grid with  $\delta g=0.2$ ,  $\delta h=0.1$ . The resulting phase-transition lines lie close together, as do their sweet spots; deviations are well below the resolution of the computing grid. Our conclusion is that  $\chi$ ,  $\chi_T$  and  $\chi_\sigma$  give comparable results.

## H. Universality and $\mathcal{F}$ -function

The function  $\mathcal{F}$  in Eq. (4) is universal, and recently values for it have been reported [33, 38]:

$$\begin{split} \mathcal{F}_{\rm free\ theory} &= \frac{\ln(2)}{8} - \frac{3\zeta(3)}{16\pi^2} \simeq 0.0638071\ \ [29] \\ \mathcal{F}_{\rm Ising}^{\rm fuzzy} &= 0.0612(5)\ \ \ (\text{fuzzy\ sphere})\ \ [33] \\ \mathcal{F}_{\rm Ising}^{4-\varepsilon} &= 0.0610 \qquad (4-\varepsilon)\ \ [38] \end{split} \tag{29}$$

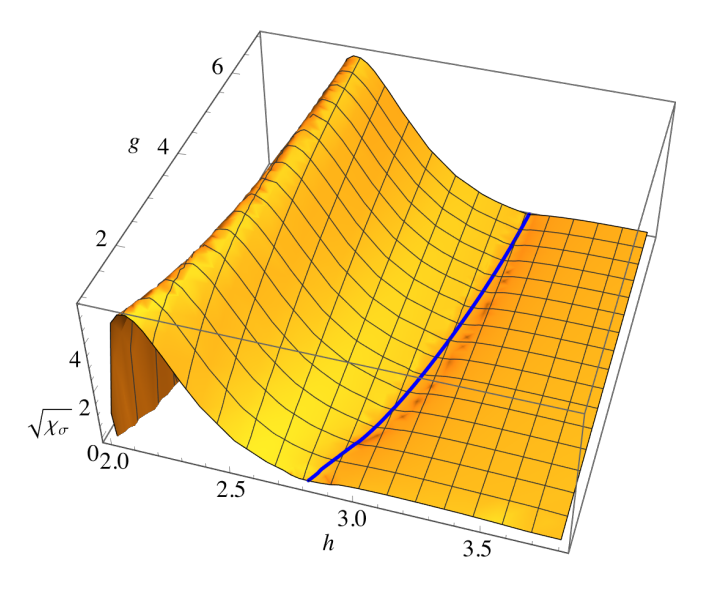


FIG. 13.  $\chi_{\sigma}$  for  $N_m^{\rm max}=15$ ; in blue the critical line. We use the same approach as in Fig. 3 for  $\chi$ , plotting the signed root  $\sqrt{\chi_{\sigma}}$ .

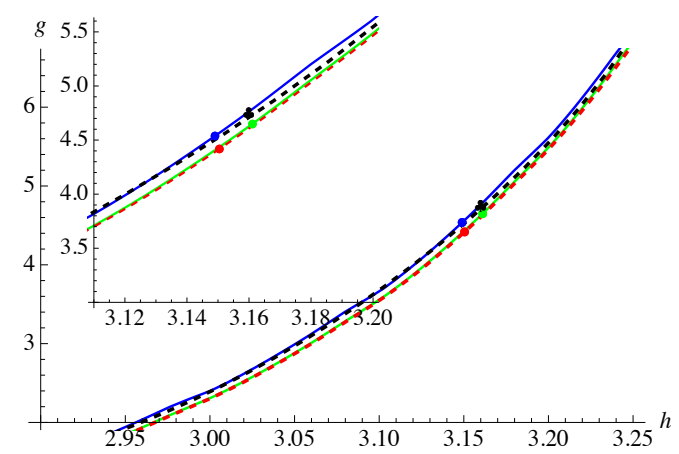


FIG. 14. As figure 6, with different denominators at size  $N_m^{\rm max}=15$ :  $\chi$  (green),  $\chi_T$  (red dashed) and  $\chi_\sigma$  (blue). In black dashed the critical line of [1], a black trefle marking its sweet spot.

Can  $\mathcal{F}$  be accessed in our approach? An obvious guess is to take  $E_{3/2}$  in units of the stress-energy tensor<sup>7</sup>,

$$\mathcal{F} \stackrel{?}{=} 3\chi_T. \tag{30}$$

At size  $N_m = 15$ , we find at the sweet spot

$$3\chi_T \approx 0.00013$$
 at  $h = 3.16$ ,  $g = 4.51$ . (31)

This value is much smaller than  $\mathcal{F}$  reported in Eq. (29). It seems that in our approach  $\chi$  may even vanish, as we tested in Fig. 15: we evaluated  $\chi$  at the sweet spot of [1], using DMRG

<sup>&</sup>lt;sup>7</sup> The number d=3 is the dimension of the stress-energy tensor.

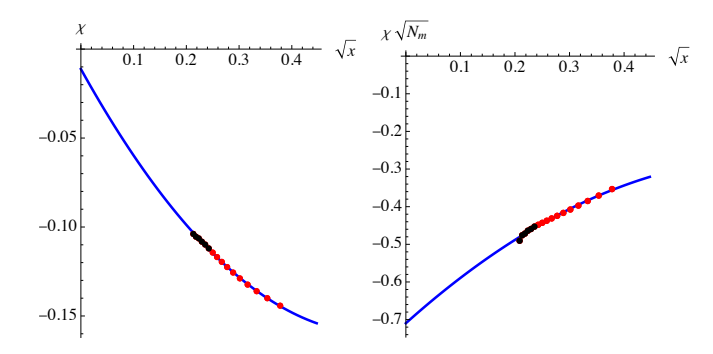


FIG. 15. Left:  $\chi$  as a function of  $\sqrt{x}$  for  $N_m$  ranging from  $N_m=6$  to  $N_m=23$ , at the sweet spot of [1], namely g=4.75, h=3.16. The black points are obtained via DMFT, and small numerical errors increase in the differences we take. (This is apparent in the last data point). To the right we show that the extrapolated value is so small, that it is consistent with a different scaling, namely that  $\chi\sqrt{N_m}$  converges for  $N_m\to\infty$ . All fits are quadratic polynomials in  $\sqrt{x}$ .

results for larger systems (the last point at  $N_m=23$  may not have converged.) By plotting both  $\chi$  and  $\chi\sqrt{N_m}$  we see that this is consistent with  $\chi=0$  at the sweet spot. So either much larger system sizes are needed to extract  $\mathcal{F}$ , or  $\chi_T$  has no connection to  $\mathcal{F}$  and vanishes at the transition. This may be expected, given that a quantum system on the fuzzy sphere is equivalent to  $S_2 \times \mathbb{R} = \mathbb{R}^3$ , and the latter should not have an anomaly.

#### IV. CONCLUSION

We have shown how the phase-transition line on the fuzzy sphere, and the sweet spot of optimal conformality can be obtained from a finite-size analysis of the ground-state energy. This is achieved by analyzing the term of relative order  $N_m^{-3/2}$  in the ground-state energy, divided by the leading term, as a function of  $N_m$ . It yields the phase-transition line of [1] and their sweet spot with good precision. While small system sizes as  $N_m=12$  already allow to locate the phase transition, the precision increases for larger  $N_m$ . A nonnegligible advantage of our approach is that it only requires to find the ground-state energy instead of the full spectrum, which is computationally fast: we need about 10 minutes for  $N_m=17$  on 8 cores.

An alternative which does not normalize by the groundstate energy is to use either the stress-energy gap, or the gap of  $\sigma$ . Both procedures take a universal normalization, give comparable results, but are computationally slightly more costly.

We hope this procedure may prove useful for locating the critical point in models as the 3-state Potts model in dimension d=3, where the transition for real couplings is first-order [7, 39, 40]. Suppose we know an approximate location of the minimum in the real plane. We can then approximate  $\chi(h,g)$  by a polynomial around this point, and search for solutions of Eq. (21) in the complex plane, near the approximate minimum.

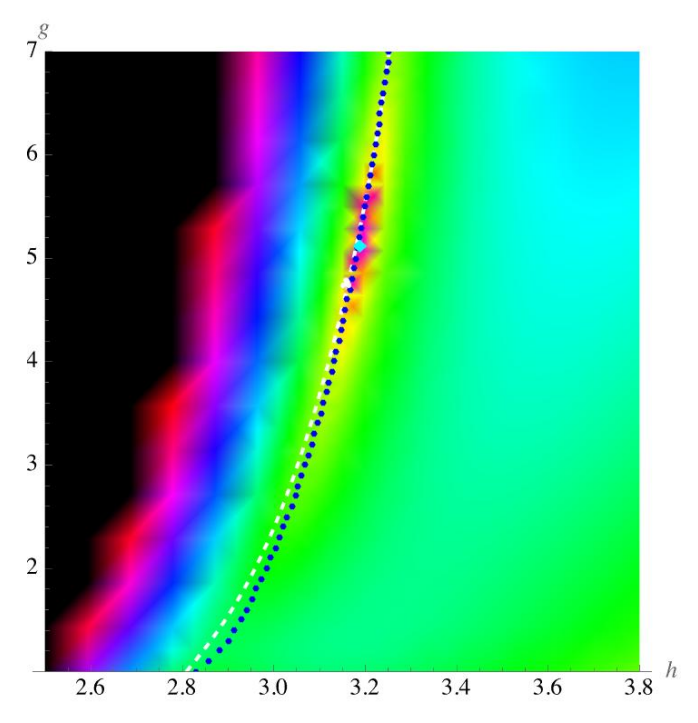


FIG. 16. The equivalent of Fig. 4, when using a polynomial in x of degree 4 for the fit, and analyzing  $-E_3/E_0$ .

#### ACKNOWLEDGMENTS

The author thanks Adam Nahum, Junchen Rong and Slava Rychkov for valuable discussions, and Yin-Chen He, Jesper Jacobsen, Adam Nahum, Zheng Zhou and Wei Zhu for feedback on the draft.

#### **Appendix A: Different extrapolation schemes**

Since the term  $E_{3/2}$  seemingly vanishes at the transition, we can try to extract the phase-transition line from a fit to a polynomial in x. A reasonable agreement was achieved by considering the term of order  $x^4$ , as is shown on Fig. 16. It finds the phase transition line, as well as the sweet spot, albeit with less precision. While we do not know whether this somehow arbitrary procedure may have a use, it indicates that the proposed approach is rather robust.

A final mark of caution: when using Eq. (17) it is important to not terminate the expansion at  $E_{3/2}$ , but to keep the two following coefficients  $E_2$  and  $E_{5/2}$ . Dropping  $E_{5/2}$  still allows one to see the phase transition, albeit only at large  $N_m$ , and with less precision; the sweet spot moves to  $h=3.2,\,g=5.3$ . Dropping both terms gives a non-sensical result.

### **CONTENTS**

- I. Introduction 1
- II. Size-dependence of the ground state energy

III.	Finite-size scaling analysis of the ground-state energy	3	IV. Conclusion	{	8
	A. Model	3			
	B. FuzzifiED	3			,
	C. Dependence of the GS energy on system size		Acknowledgments		5
	D. Implementation	4			
E. Results for the location of the critical point		4	A. Different extrapolation schemes		9
	F. Curvature scaling		71. Different extrapolation senemes		
	G. Alternative normalizations	6			
	H. Universality and $\mathcal{F}$ -function	7	References	Ģ	(

- [1] W. Zhu, C. Han, E. Huffman, J.S. Hofmann and Y.-C. He, *Uncovering conformal symmetry in the 3d Ising transition: State-operator correspondence from a quantum fuzzy sphere regularization*, Phys. Rev. X **13** (2023) 021009, arXiv:2210.13482.
- [2] Z. Zhou and Y.-C. He, A new series of 3d CFTs with Sp(n) global symmetry on fuzzy sphere, (2024), arXiv:2410.00087.
- [3] A. Dey, L. Herviou, C. Mudry and A.M. Läuchli, *Conformal data for the O(3) Wilson-Fisher CFT from fuzzy sphere realization of quantum rotor model*, (2025), arXiv:2510.09755.
- [4] Z. Zhou, D. Gaiotto and Y.-C. He, Free Majorana fermion meets gauged Ising conformal field theory on the fuzzy sphere, (2025), arXiv:2509.08038.
- [5] Y.-C. He, Free real scalar CFT on fuzzy sphere: spectrum, algebra and wavefunction ansatz, (2025), arXiv:2506.14904.
- [6] Z. Zhou, C. Wang and Y.-C. He, Chern-Simons-matter conformal field theory on fuzzy sphere: Confinement transition of Kalmeyer-Laughlin chiral spin liquid, (2025), arXiv:2507.19580.
- [7] S. Yang, Y.-G. Yue, Y. Tang, C. Han, W. Zhu and Y. Chen, Microscopic study of 3d Potts phase transition via fuzzy sphere regularization, Phys. Rev. B 112 (2025) 024436, arXiv:2501.14320.
- [8] R. Fan, J. Dong and A. Vishwanath, Simulating the non-unitary Yang-Lee conformal field theory on the fuzzy sphere, (2025), arXiv:2505.06342.
- [9] E.A. Cruz, I.R. Klebanov, G. Tarnopolsky and Y. Xin, Yang-Lee quantum criticality in various dimensions 2025, arXiv:2505.06369.
- [10] J.E. Miro and O. Delouche, Flowing from the Ising model on the fuzzy sphere to the 3D Lee-Yang CFT, JHEP 10 (2025) 037, arXiv:2505.07655.
- [11] M. Reehorst, S. Rychkov, D. Simmons-Duffin, B. Sirois, N. Su and B. van Rees, *Navigator function for the conformal boot*strap, SciPost Phys. 11 (2021) 072.
- [12] D. Poland, S. Rychkov and A. Vichi, The conformal bootstrap: Theory, numerical techniques, and applications, Rev. Mod. Phys. 91 (2019) 015002.
- [13] S. El-Showk, M. F. Paulos, D. Poland, S. Rychkov, D. Simmons-Duffin and A. Vichi, Solving the 3d Ising model with the conformal bootstrap ii. c-minimization and precise critical exponents, J. Stat. Phys. 157 (2014) 869–914, arXiv:1403.4545.
- [14] S. El-Showk, M.F. Paulos, D. Poland, S. Rychkov, D. Simmons-Duffin and A. Vichi, Solving the 3D Ising model with the conformal bootstrap, Phys. Rev. D 86 (2012) 025022.
- [15] S.M. Chester, W. Landry, J. Liu, D. Poland, D. Simmons-Duffin, N. Su and A. Vichi, *Carving out ope space and precise* O(2) model critical exponents, (2019), arXiv:1912.03324.
- [16] G. Fardelli, A.L. Fitzpatrick and E. Katz, Constructing the infrared conformal generators on the fuzzy sphere, (2024),

- arXiv:2409.02998.
- [17] R. Fan, Note on explicit construction of conformal generators on the fuzzy sphere, (2024), arXiv:2409.08257.
- [18] H.W.J. Blöte, J.L. Cardy and M.P. Nightingale, Conformal invariance, the central charge, and universal finite size amplitudes at criticality, Phys. Rev. Lett. 56 (1986) 742–745.
- [19] J. Cardy, Conformal invariance and statistical mechanics, in E. Brézin and J. Zinn-Justin, editors, Fields, strings and critical phenomena, Volume XLIX of Les Houches, école d'été de physique théorique 1988, North Holland, Amsterdam, 1988.
- [20] J.L. Jacobsen and K.J. Wiese, Lattice realization of complex CFTs: Two-dimensional Potts model with Q > 4 states, Phys. Rev. Lett. 133 (2024) 077101, arXiv:2402.10732.
- [21] A.B. Zamolodchikov, "Irreversibility" of the flux of the renormalization group in a 2D field theory, Pis'ma Zh. Eksp. Theor. Fiz. 43 (1986) 565–567, JETP Lett. 43 (1986) 730.
- [22] S. Deser and A. Schwimmer, Geometric classification of conformal anomalies in arbitrary dimensions, Phys. Lett. B 309 (1993) 279–284.
- [23] M.J. Duff, *Twenty years of the Weyl anomaly*, Classical and Quantum Gravity **11** (1994) 1387.
- [24] Z. Komargodski and A. Schwimmer, On renormalization group flows in four dimensions, JHEP 2011 (2011) 99.
- [25] J.L. Cardy, Is there a c-theorem in four dimensions?, Phys. Lett. B 215 (1988) 749–752.
- [26] D.L. Jafferis, I.R. Klebanov, S.S. Pufu and B.R. Safdi, *Towards the F-theorem:*  $\mathcal{N}=2$  *field theories on the three-sphere*, JHEP **2011** (2011) 102.
- [27] R.C. Myers and A. Sinha, *Holographic c-theorems in arbitrary dimensions*, JHEP **2011** (2011) 125, arXiv:1011.5819.
- [28] D.L. Jafferis, The exact superconformal R-symmetry extremizes Z, JHEP 2012 (2012) 159, arXiv:1012.3210.
- [29] I.R. Klebanov, S.S. Pufu and B.R. Safdi, F-theorem without supersymmetry, JHEP 2011 (2011) 38, arXiv:1105.4598.
- [30] M.P. Hertzberg and F. Wilczek, *Some calculable contributions to entanglement entropy*, Phys. Rev. Lett. **106** (2011) 050404.
- [31] H. Liu and M. Mezei, A refinement of entanglement entropy and the number of degrees of freedom, JHEP 2013 (2013) 162, arXiv:1202.2070.
- [32] H. Casini and M. Huerta, Renormalization group running of the entanglement entropy of a circle, Phys. Rev. D 85 (2012) 125016.
- [33] L. Hu, W. Zhu and Y.-C. He, Entropic F-function of 3D Ising conformal field theory via the fuzzy sphere regularization, (2024), arXiv:2401.17362.
- [34] Z. Zhou, Fuzzified: Julia package for numerics on the fuzzy sphere, (2025), arXiv:2503.00100.
- [35] A.W.W. Ludwig and J.L. Cardy, Perturbative evaluation of the conformal anomaly at new critical points with applications to random systems, Nucl. Phys. B 285 (1987) 687–718.

- [36] M. Hogervorst, S. Rychkov and B.C. van Rees, *Truncated conformal space approach in d dimensions: A cheap alternative to lattice field theory?*, Phys. Rev. D **91** (2015) 025005.
- [37] A.M. Läuchli, L. Herviou, P.H. Wilhelm and S. Rychkov, Exact diagonalization, matrix product states and conformal perturbation theory study of a 3d Ising fuzzy sphere model, (2025), arXiv:2504.00842.
- [38] S. Giombi and I.R. Klebanov, Interpolating between a and F,
- JHEP **2015** (2015) 117.
- [39] A. K. Hartmann, Calculation of partition functions by measuring component distributions, Phys. Rev. Lett. **94** (2005) 050601.
- [40] S.M. Chester and N. Su, *Upper critical dimension of the 3-state Potts model*, (2022), arXiv:2210.09091.